

Fractionalized Kohn-Sham ansatz for strongly-correlated electrons

Bo Zhao,¹ Jingyu Zhao,² Zheng Zhu,³ Jian Wu,^{1,4} and Zheng Liu^{5,*}

¹*State Key Laboratory of Low Dimensional Quantum Physics,
Department of Physics, Tsinghua University, Beijing 100084, China*

²*Institute for Advanced Study, Tsinghua University, Beijing 100084, China*

³*Kavli Institute for Theoretical Sciences, University of Chinese Academy of Sciences, Beijing 100190, China*

⁴*Frontier Science Center for Quantum Information, Beijing, China.*

⁵*School of Physics, Beihang University, Beijing 100191, China*

We propose to expand the territory of density functional theory to strongly-correlated electrons by reformulating the Kohn-Sham ansatz in the representation of fractionalized particles. We call it the “KS* ansatz”. Using inhomogeneous t - J chains as a test bed, we show that the KS* ansatz with simple local density approximation is able to achieve accurate ground state energy and density distribution comparable to the density matrix renormalization group method, while the computational complexity is much lower.

The success of density functional theory (DFT) [1, 2] for first-principles electronic structure calculations is built upon the Kohn-Sham (KS) ansatz [3], which asserts that a noninteracting auxiliary system with a properly chosen exchange-correlation (XC) potential has the same ground-state (GS) density as the original interacting electrons. Together with the local density approximation (LDA) or its improved versions to the XC potential, the KS approach is proved to work well for a wide range of condensed matters and molecular systems [4]. However, it is also known to fail in systems dominated by electron-electron interactions [5, 6]. The strong quantum correlation makes such systems lack resemblance to a noninteracting electron gas.

Tremendous efforts have been made to expand the territory of first-principles calculation to the strong-correlation regime, either by improving the XC potential [7–10] or hybridizing DFT with other many-body techniques [11–14]. In this Letter, we aim to explore a new direction by highlighting one prominent feature of strong correlation, namely the emergence of exotic quasi-particles as a fraction of the electrons (For a recent overview, see [15] and references therein). Instead of further upgrading interaction corrections within the standard KS setup, we propose to construct new types of non-interacting auxiliary systems consisting of fractionalized particles rather than electrons, which we term as “fractionalized KS (KS*) ansatz”.

Theoretically, the power of fractionalization lies in the possibility to transform strongly-correlated electrons into weakly-correlated quasi-particles. A well-known example is the spin-charge separation in a Luttinger liquid [16], and more and more strongly-correlated systems are becoming describable within this framework (See e.g. Parts II and IV in [15]). The expectation is that a well-chosen

fractionalization scheme will largely reduce the complexity of the XC potential, such that satisfactory results could be achieved at the simple and efficient LDA level.

The general concept of KS* ansatz opens new possibilities to tackle different strongly-correlated phases within DFT, but the design of the fractionalized auxiliary system and the density function(al)s requires theoretical thoughts and numerical tests in a case-by-case way. To implement this idea in an explicit strongly-correlated system, we choose the 1D t - J model as the first example. We write the Hamiltonian as

$$\hat{H} = \hat{H}_0 + \hat{H}_{int}, \quad (1)$$

with

$$\begin{aligned} \hat{H}_0 &= -t \sum_{i\sigma} (c_{i\sigma}^\dagger c_{i+1\sigma} + H.c.) + \sum_i V_i \hat{n}_i \\ \hat{H}_{int} &= J \sum_i (\hat{S}_i \cdot \hat{S}_{i+1} - \frac{\hat{n}_i \hat{n}_{i+1}}{4}). \end{aligned} \quad (2)$$

The operator $c_{i\sigma}^\dagger$ creates an electron at site i with spin σ , \hat{S}_i is the site spin operator, $\hat{n}_i = \sum_{\sigma} c_{i\sigma}^\dagger c_{i\sigma}$ is the electron number operator, and V_i is the external potential.

The t - J model arises from a downfold of the Hubbard model at the large- U limit, which is thus constrained by the no-double-occupancy condition:

$$n_i \leq 1. \quad (3)$$

Properly treating this constraint is essential to understand doped Mott insulators [17]. Hole doping is measured from the half-filling $n_i = 1$ limit, i.e. N_h holes correspond to a total electron number $N_s - N_h$, where N_s is the number of sites.

We have several motivations to take a detour from the full Hamiltonian of interacting electrons to such an

effective lattice model. Firstly, the strongly-correlated regime of interacting electrons is typically accessed under a strong lattice potential, e.g. in d,f -electron materials, where the lattice model represents a more efficient description than the plane-wave continuum model [18]. Secondly, while the more familiar Hubbard model still has a perturbative regime when the onsite interaction U is small, the t - J model focuses on the strong-correlation regime, as explicitly reflected by the no-double-occupancy constraint [17]. Thirdly, despite the long-lasting challenge toward a thorough understanding of the 2D t - J model and its implication on high- T_c cuprate superconductors [17], the Luttinger liquid behavior in 1D is quantitatively solvable, both analytically [19] and numerically via the density matrix renormalization group (DMRG) method [20]. Therefore, the performance of our new ansatz can be systematically tested. Once encouraging results have been obtained from this transparent effective model, we can move on to more complicated setups, and ultimately toward realistic materials.

Before invoking fractionalization, let us first revisit the standard KS ansatz. For the discrete lattice model, we compact the density distribution as a vector: $\vec{n} \triangleq (n_1, n_2, n_3, \dots)$. The KS ansatz can be rephrased as:

(KS) *Once t and J are fixed in Eq.(2), a so-called XC energy function $E_{xc}(\vec{n})$ in principle exists, such that solving the auxiliary Hamiltonian:*

$$\hat{H}_{KS} = \hat{H}_0 + \hat{V}_{xc} \quad (4)$$

with

$$\hat{V}_{xc} = \sum_i \frac{\partial E_{xc}}{\partial n_i} \hat{n}_i \quad (5)$$

gives the exact GS density. The GS expectation value of \hat{H}_0 of the auxiliary system plus E_{xc} gives the exact GS energy.

LDA renders an approximated but straightforward construction of $E_{xc}(\vec{n})$ by referring to the XC energy per electron $\epsilon_{xc}(n)$ of the homogeneous chain, i.e. $V_i \equiv 0$ and $n_i = n$. The LDA formula is

$$E_{xc}(\vec{n}) \approx \sum_i n_i \epsilon_{xc}(n_i). \quad (6)$$

Extending the formula to spin-polarized cases is straightforward, but we will focus on the nonmagnetic regime in the present work.

The required information to wrap up the computation is then reduced to $\epsilon_{xc}(n)$ of the homogeneous chain. Like the role of quantum Monte Carlo played for the homogeneous electron gas [21], DMRG can be used to give an accurate measure of the total energy per electron of the

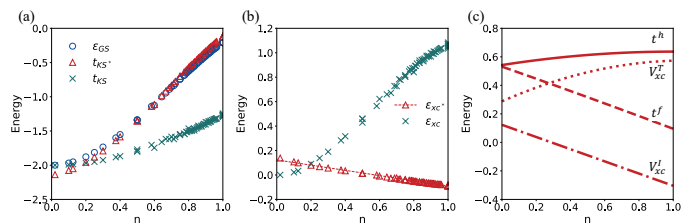


FIG. 1. Homogeneous density dependence of (a) ϵ_{GS} , t_{KS} , t_{KS}^* ; (b) ϵ_{xc} , ϵ_{xc}^* ; and (c) t^h , t^f , V_{xc}^T , V_{xc}^I . See context for the definitions. Data shown in (a) and (b) are collected from calculations on finite N_s -site chains ($N_s=10\sim 50$) containing different number of holes under the periodic boundary condition (PBC). t_{KS}^* in (a) is obtained by using the LDA parameters $A = 0.45$, $B = -0.05$. The dashed line in (b) is the linear fitting $\epsilon_{xc}^* = -0.21n_i + 0.12$.

homogeneous chain [ϵ_{GS} , blue circles in Fig. 7(a)]. The kinetic energy per electron of the noninteracting chain [t_{KS} , green crosses in Fig. 7(a)] can be easily calculated. By definition, $\epsilon_{xc} = \epsilon_{GS} - t_{KS}$ [green crosses in Fig. 7(b)].

For all the numerical calculations, we treat t as the energy unit, and J is fixed to be 0.3. We note that $J/t = 0.3$ is the common ratio employed for numerical study of t - J models [22–25] due to connections to the realistic parameters of cuprates (See e.g. Sec. II of [17]). DMRG computational details are given in the Supplementary Materials (SM).

One quick observation is that t_{KS} becomes significantly lower than ϵ_{GS} when n increases, reflecting that the antiferromagnetic superexchange frustrates the motion of electrons. The positive ϵ_{xc} and negative t_{KS} largely cancel each other as n approaches 1. We have tested to solve Eqs. (4-6) self-consistently for several inhomogeneous density profiles. The performance is poor (Fig. S1). It also requires additional advanced techniques, e.g. Gutzwiller projection, to take into account the no-double-occupancy constraint within this framework [26, 27]. All these issues make it cumbersome to proceed along the conventional KS scheme.

We now switch to the KS* ansatz. The starting point is that the general Luttinger liquid behavior of 1D interacting electrons asserts spin-charge separation. Accordingly, we assume a fractionalized auxiliary system consisting of (i) spinless particles each carrying a positive elementary charge (holons); and (ii) neutral spin-1/2 particles (spinons). The holons and spinons move with their own velocities. We write their hopping amplitudes as t_i^h and t_i^f , respectively, which typically differ from t in \hat{H}_0 , due to the renormalization effect of \hat{H}_{int} . The external potential V_i couples to the charge degree of freedom, i.e. holons. Besides, we add a XC potential V_{xc} as in

the conventional KS scheme. \hat{H}_{int} manifests in V_{xc} , as well as t_i^h and t_i^f . The three quantities are considered to be functions of the density distribution. The no-double-occupancy constraint means that each site is occupied either by a holon or a spinon. Therefore, the total number of holons and spinons at each site should always be one, which conveniently transforms the inequality constraint into the condition $\langle h_i^\dagger h_i + \sum_\sigma f_{i\sigma}^\dagger f_{i\sigma} \rangle = 1$, which can be enforced by introducing Lagrange multipliers λ_i , and by self-consistently determining λ_i as a local chemical potential. Formally, we write a non-interacting Hamiltonian as following:

$$\begin{aligned} \hat{H}_{KS^*} = & - \sum_i t_i^h(\bar{n}) h_i^\dagger h_{i+1} - \sum_{i\sigma} t_i^f(\bar{n}) f_{i\sigma}^\dagger f_{i+1\sigma} + H.c. \\ & + \sum_i (V_i + V_{xc,i}(\bar{n}))(1 - h_i^\dagger h_i) \\ & + \sum_i \lambda_i (h_i^\dagger h_i + \sum_\sigma f_{i\sigma}^\dagger f_{i\sigma} - 1), \end{aligned} \quad (7)$$

in which h_i^\dagger ($f_{i\sigma}^\dagger$) creates a holon (spinon). Note that $1 - h_i^\dagger h_i = \hat{n}_i$ within the no-double-occupancy subspace, consistent with our definition of hole doping concentrations. To keep the fermionic statistics of electrons, we assign $f_{i\sigma}$ as a fermion operator and h_i as a hard-core boson operator. In practical calculations, h_i will be transformed into a fermion operator via the 1D Jordan-Wigner transformation (See Sec. IV of SM).

Based on Eq.(7), we propose the KS* ansatz:

(KS*) Once t and J are fixed in Eq.(2), function forms of $t_i^{h(f)}(\bar{n})$ and $V_{xc,i}(\bar{n})$ in principle exist, such that solving Eq. (7) gives the exact GS density. The exact GS energy can be obtained from a corresponding energy function, which links to Eq. (7) via the variational principle.

The proposal is intuitively backed by the Luttinger liquid behavior of 1D interacting electrons [28]. Most relevantly, an elegant slave-particle construction $c_{i\sigma} = h_i^\dagger f_{i\sigma}$ is known (See e.g. Sec. XIII of [17]) to transform Eq. (2) into:

$$\begin{aligned} \hat{H}_0 = & -t \sum_{i\sigma} h_{i+1}^\dagger h_i f_{i\sigma}^\dagger f_{i+1\sigma} + H.c. + \sum_i V_i \hat{n}_i \\ \hat{H}_{int} = & -\frac{J}{2} \sum_{i\sigma\sigma'} f_{i\sigma}^\dagger f_{i+1\sigma} f_{i+1\sigma'}^\dagger f_{i\sigma'} \end{aligned} \quad (8)$$

Then, a mean-field treatment leads to the following

noninteracting Hamiltonian[29, 30]:

$$\begin{aligned} \hat{H}_{MF^*} = & - t \sum_{i\sigma} \langle f_{i+1\sigma}^\dagger f_{i\sigma} \rangle h_i^\dagger h_{i+1} \\ & - \sum_{i\sigma\sigma'} \left(\frac{J}{2} \langle f_{i+1\sigma'}^\dagger f_{i\sigma'} \rangle + t \langle h_{i+1}^\dagger h_i \rangle \right) f_{i\sigma}^\dagger f_{i+1\sigma} \\ & + H.c. + \sum_i V_i \hat{n}_i \end{aligned} \quad (9)$$

The relation between \hat{H}_{MF^*} and \hat{H}_{KS^*} is analogous to that between the Hartree-Fock mean-field treatment of the electron gas and the KS equations. For the electron gas, it is well known that the KS ansatz not only renders a formal exactification, but also in many cases practically surpasses the mean field in accuracy [4]. We will see that the KS* ansatz retains these advantages.

\hat{H}_{KS^*} contains three density functions. In addition to the XC potential V_{xc} , we additionally introduce density dependence to $t_i^{h(f)}$. Physically, it means that \hat{H}_{int} also manifests in the motion of the fractionalized particles, as it should do. According to \hat{H}_{MF^*} ,

$$\begin{aligned} t_i^h & = t \sum_\sigma \langle f_{i+1\sigma}^\dagger f_{i\sigma} \rangle \\ t_i^f & = \frac{J}{2} \sum_{\sigma'} \langle f_{i+1\sigma'}^\dagger f_{i\sigma'} \rangle + t \langle h_{i+1}^\dagger h_i \rangle. \end{aligned} \quad (10)$$

However, we find that directly applying this formula tends to result in unrealistic oscillating $t_i^{h(f)}$ when n_i is inhomogeneous. The failure can be most easily seen in a half-filled 4-site chain with the open boundary condition (OBC), for which \hat{H}_{MF^*} predicts an incorrect valence-bond-solid state (See Sec. II of SM). Numerical comparisons between DMRG and \hat{H}_{MF^*} GS's on several inhomogeneous density profiles also indicate noticeable errors (Fig. S2).

Instead, we invoke LDA to $\langle h_i^\dagger h_{i+1} \rangle$ and $\langle f_{i\sigma}^\dagger f_{i+1\sigma} \rangle$, and require the density functions recover the behavior of the mean-field definition at the homogeneous limit (See Sec. III of SM) in two aspects:(i) when $n_i = 1$, $\langle h_i^\dagger h_{i+1} \rangle = 0$, $\langle f_{i\sigma}^\dagger f_{i+1\sigma} \rangle = \frac{1}{\pi}$; and (ii) when n_i approaches 1 from below, $\delta \langle h_i^\dagger h_{i+1} \rangle \propto 1 - n_i$, $\delta \langle f_{i\sigma}^\dagger f_{i+1\sigma} \rangle \propto (1 - n_i)^2$. These constraints lead to:

$$\begin{aligned} \langle h_i^\dagger h_{i+1} \rangle_{LDA} & \approx A(1 - n_i) \\ \langle f_{i\sigma}^\dagger f_{i+1\sigma} \rangle_{LDA} & \approx \frac{1}{\pi} + B(1 - n_i)^2, \end{aligned} \quad (11)$$

in which A and B are two LDA parameters. Substituting Eq. (11) back into Eq. (10) decides the LDA forms of $t_i^{h(f)}$.

The values of A and B are determined as follows. Different choices of A and B lead to different kinetic energies

of the KS* auxiliary system (t_{KS^*}), and in turn different XC energies (ϵ_{xc^*} , as defined by the difference between ϵ_{GS} and t_{KS^*}). In this sense, A and B tune the partition of the GS energy into the kinetic and potential parts, which is non-unique. In Fig. S3, we plot t_{KS^*} and ϵ_{xc^*} obtained from several values of A and B , as well as from the rigorous mean-field definition of $\langle h_i^\dagger h_{i+1} \rangle$ and $\langle f_{i\sigma}^\dagger f_{i+1\sigma} \rangle$. Note that for homogeneous chains, they all consistently reproduce the exact GS energy. Testing calculations on inhomogeneous chains show that $A = 0.45$ and $B = -0.05$ generally perform well. A phenomenological understanding is that this choice makes t_{KS^*} captures a predominant part of ϵ_{GS} , and ϵ_{xc^*} shows a simple linear dependence on n [Figs. 7(a,b)]. In all the calculations below we will fix $A = 0.45$ and $B = -0.05$ without further fine tuning.

\hat{H}_{KS^*} becomes formally exact by rederiving it as a variational minimum of the GS energy, i.e. $\delta E_{GS}/\delta \langle \Psi_{KS^*} | = 0$, where $\langle \Psi_{KS^*} |$ is the complex conjugate of the GS wavefunction of the KS* auxiliary system.

Special attentions should be paid to the kinetic energy, since $t_i^{f(h)}$ is now density dependent. We have:

$$\begin{aligned} \frac{\delta T_{KS^*}}{\delta \langle \Psi_{KS^*} |} &= \hat{T}_{KS^*} | \Psi_{KS^*} \rangle \\ &- \langle \Psi_{KS^*} | \frac{\partial \hat{T}_{KS^*}}{\partial n_i} | \Psi_{KS^*} \rangle \hat{n}_i | \Psi_{KS^*} \rangle. \end{aligned} \quad (12)$$

The second term on the right-hand side contributes a kinetically generated XC potential, which we denote as $V_{xc,i}^T \equiv \langle \Psi_{KS^*} | \frac{\partial \hat{T}_{KS^*}}{\partial n_i} | \Psi_{KS^*} \rangle$. Under LDA, an explicit form can be given:

$$\begin{aligned} V_{xc,i}^T &\approx - 2 \langle h_i^\dagger h_{i+1} \rangle_{LDA} \frac{dt_i^h}{dn} \Big|_{n=n_i, LDA} \\ &- 4 \langle f_{i\sigma}^\dagger f_{i+1\sigma} \rangle_{LDA} \frac{dt_i^f}{dn} \Big|_{n=n_i, LDA}. \end{aligned} \quad (13)$$

In addition, $\delta E_{xc^*}/\delta \langle \Psi_{KS^*} |$ leads to the common interaction generated xc potential, which we denote as $V_{xc,i}^I$. The LDA form is:

$$V_{xc,i}^I \approx \epsilon_{xc^*}(n_i) + n_i \frac{d\epsilon_{xc^*}}{dn} \Big|_{n=n_i}. \quad (14)$$

The complete XC potential entering Eq. (7) is $V_{xc} = V_{xc}^T + V_{xc}^I$.

We plot all the density functions in Fig. 7(c). Plugging these into \hat{H}_{KS^*} , self-consistent calculations can be performed to solve the t - J chain with arbitrary input of lattice potentials ($V_{i=1,\dots,N_s}$) and number of doped holes (N_h). Figure 8 shows the computational flow chart, and Sec. IV of SM contains more implementation details.

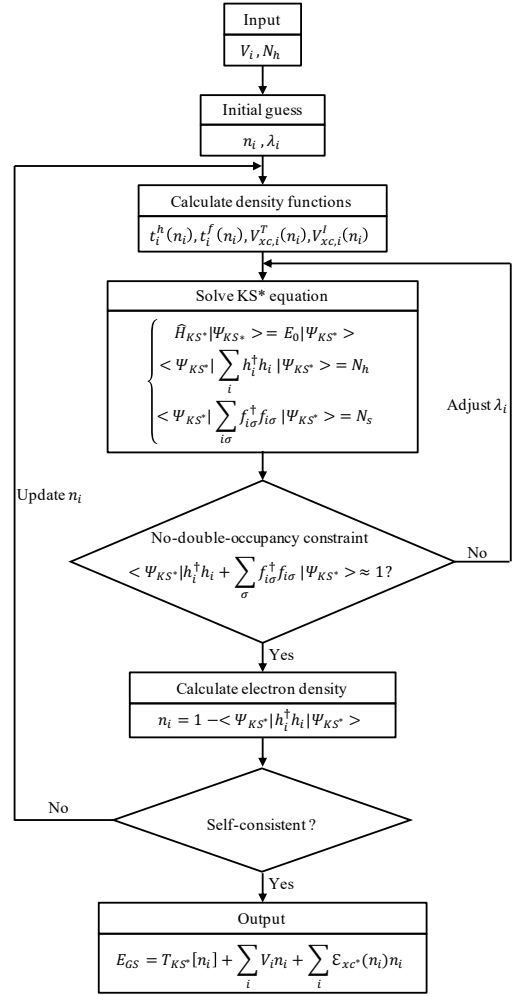


FIG. 2. Schematic representation of the self-consistent iteration for solution of \hat{H}_{KS^*} .

Figures 5(a-c) summarize the 1-hole GS energies in three representative cases with inhomogeneous density: (a) an OBC chain; (b) a PBC chain subject to a single-site impurity potential; (c) a PBC chain subject to a periodic potential. E_{GS} is plotted as a function of (a) chain length (N_s), (b) impurity strength (V_{imp}) and (c) potential period (N_p), respectively. For all the cases, we find that the KS* formalism is able to well trace the DMRG GS energy. More importantly, Figs. 5(d-f) decompose the calculated E_{GS} into T_{KS^*} , E_{xc^*} and $E_{ext} \equiv \sum_i V_i n_i$ within the KS* scheme. Clearly, the total energy contains a non-negligible contribution from the XC energy, and is crucial to obtain an accurate E_{GS} , which however is missing in the slave-particle mean-field framework.

For each case, we select a parameter point, and plot the GS density distribution in Figs. 5(g-i). We have also calculated the 2-hole, 3-hole and 9-hole GS density distributions in Fig. 10. All the results show excellent agreement

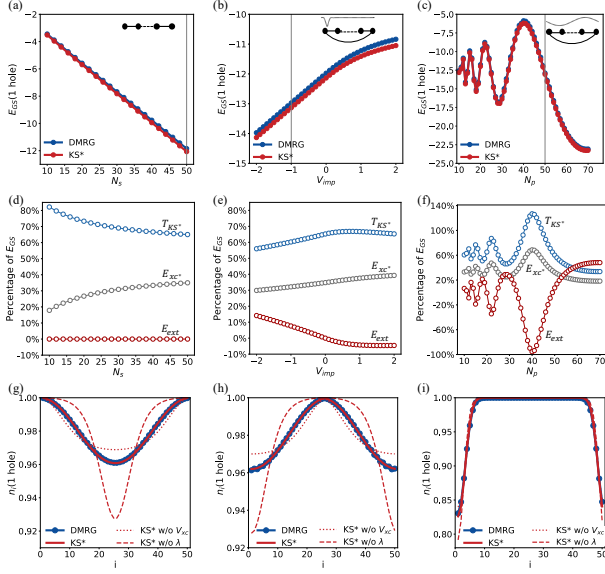


FIG. 3. The 1-hole GS energy of (a) a N_s -site OBC chain; (b) a 50-site PBC chain subject to a single-site impurity potential $V_i = \delta_{i1} V_{imp}$; and (c) a 50-site PBC chain subject to a periodic potential $V_i = \cos(2\pi i/N_p)$. The vertical grey lines mark the parameter for the density plot in the bottom panels. (d-f) Decomposition of the calculated E_{GS} in the top panels into T_{KS^*} , E_{exc^*} and $E_{ext} \equiv \sum_i V_i n_i$ within the KS^* scheme. (g-i) The 1-hole GS density distributions corresponding to the setups of the top panels. For (e), the impurity site is plotted as the center of the chain.

with DMRG. While the local chemical potential λ_i does not directly contribute to the energy, it is found to play an important role in improving the density description.

The multi-hole energy comparison and decomposition are shown in Sec. V of SM. It is worth mentioning that the DMRG algorithm as implemented in ITensors [31, 32] takes more than 1 hour to solve a 50-site t - J chain using a 24-core HPC node, while the KS^* iteration finishes typically within 1 min on a laptop without parallel optimization.

In summary, we show that a DFT iteration algorithm formulated using the representation of emergent particles solves the 1D t - J model with accuracy comparable to DMRG and much lower computational cost. The choice of an unconventional KS auxiliary system represents the key to extend the power of DFT to solve strongly-correlated multiparticle quantum systems. For general spatial dimensions, one additional complexity is the emergent gauge field associated with fractionalization [25, 29, 30, 33]. We note that a recent closely-related achievement is the demonstration of composite-fermion DFT for fractional quantum Hall systems [34–36], which incorporates emergent gauge interactions in

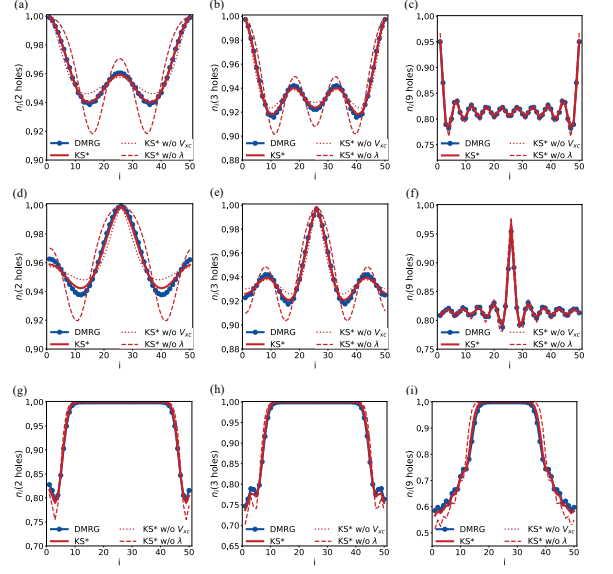


FIG. 4. The 2-, 3- and 9-hole GS density distributions of (a-c) a 50-site OBC chain; (d-f) a 50-site PBC chain subject to a single-site impurity potential; and (g-i) a 50-site PBC chain subject to a periodic potential $V_i = \cos(2\pi i/N_p)$.

the KS auxiliary system by using the density-dependent flux attachment technique. Combining this technique with the KS^* ansatz will be a novel step to solve higher-dimensional strongly-correlated models, and one step further, when we seek for DFT descriptions of realistic strongly-correlated materials, such as high- T_c cuprates. Another complexity is the competition of various distinct phases. A feasible strategy is similar to determining the mean-field phase diagram of a strongly-correlated system. Supposing we now have a family of KS^* equations, each reproducing the GS energy of a specific phase accurately. The lowest-energy solution thus selects the stable phase. On the whole, new versions of KS ansatz covering both fractionalized particles and emergent gauge fields are expected to carry DFT into a new realm.

We would like to thank Z.Y. Weng for valuable discussions. This work is supported by National Natural Science Foundation of China (Grant Nos. 12374062, 92365201, 12074375), National Key R&D Program of China (2023YFA1406400) and the Fundamental Research Funds for the Central Universities.

* zliu23@buaa.edu.cn

- [1] P. Hohenberg and W. Kohn, Inhomogeneous electron gas, *Phys. Rev. B* **136**, B864 (1964).
- [2] R. O. Jones, Density functional theory: Its origins, rise to

- prominence, and future, *Rev. Mod. Phys.* **87**, 897 (2015).
- [3] W. Kohn and L. J. Sham, Self-consistent equations including exchange and correlation effects, *Phys. Rev.* **140**, A1133 (1965).
- [4] W. Kohn, Nobel lecture: Electronic structure of matter—wave functions and density functionals, *Rev. Mod. Phys.* **71**, 1253 (1999).
- [5] P. Gori-Giorgi, M. Seidl, and G. Vignale, Density-functional theory for strongly interacting electrons, *Phys. Rev. Lett.* **103**, 166402 (2009).
- [6] F. Malet and P. Gori-Giorgi, Strong correlation in Kohn-Sham density functional theory, *Phys. Rev. Lett.* **109**, 246402 (2012).
- [7] S. Kummel and L. Kronik, Orbital-dependent density functionals: Theory and applications, *Rev. Mod. Phys.* **80**, 3 (2008).
- [8] J. P. Perdew and K. Schmidt, Jacob’s ladder of density functional approximations for the exchange-correlation energy, *AIP Conf. Proc.* **577**, 1 (2001).
- [9] J. Sun, A. Ruzsinszky, and J. P. Perdew, Strongly constrained and appropriately normed semilocal density functional, *Phys. Rev. Lett.* **115**, 036402 (2015).
- [10] J. Kirkpatrick, B. McMorro, D. H. P. Turban, A. L. Gaunt, J. S. Spencer, A. G. D. G. Matthews, A. Obika, L. Thiry, M. Fortunato, D. Pfau, L. R. Castellanos, S. Petersen, A. W. R. Nelson, P. Kohli, P. Mori-Sánchez, D. Hassabis, and A. J. Cohen, Pushing the frontiers of density functionals by solving the fractional electron problem, *Science* **374**, 1385 (2021).
- [11] G. Kotliar, S. Y. Savrasov, K. Haule, V. S. Oudovenko, O. Parcollet, and C. A. Marianetti, Electronic structure calculations with dynamical mean-field theory, *Rev. Mod. Phys.* **78**, 865 (2006).
- [12] J. M. Tomczak, P. Liu, A. Toschi, G. Kresse, and K. Held, Merging GW with DMFT and non-local correlations beyond, *Eur. Phys. J. Spec. Top.* **226**, 2565 (2017).
- [13] B. Kang, P. Semon, C. Melnick, G. Kotliar, and S. Choi, ComDMFT v.2.0: Fully Self-Consistent ab initio GW+EDMFT for the Electronic Structure of Correlated Quantum Materials, [arXiv:2310.04613](https://arxiv.org/abs/2310.04613).
- [14] G. Onida, L. Reining, and A. Rubio, Electronic excitations: density-functional versus many-body Green’s-function approaches, *Rev. Mod. Phys.* **74**, 601 (2002).
- [15] S. Sachdev, *Quantum Phases of Matter* (Cambridge University Press, 2023).
- [16] J. Voit, A brief introduction to luttinger liquids, *AIP Conf. Proc.* **544**, 309 (2000).
- [17] P. A. Lee, N. Nagaosa, and X.-G. Wen, Doping a mott insulator: Physics of high-temperature superconductivity, *Rev. Mod. Phys.* **78**, 17 (2006).
- [18] K. Capelle and V. L. Campo Jr, Density functionals and model hamiltonians: Pillars of many-particle physics, *Physics Reports* **528**, 91 (2013).
- [19] E. H. Lieb and F. Y. Wu, Absence of mott transition in an exact solution of the short-range, one-band model in one dimension, *Phys. Rev. Lett.* **20**, 1445 (1968).
- [20] U. Schollwöck, The density-matrix renormalization group, *Rev. Mod. Phys.* **77**, 259 (2005).
- [21] D. M. Ceperley and B. J. Alder, Ground state of the electron gas by a stochastic method, *Phys. Rev. Lett.* **45**, 566 (1980).
- [22] A. Moreno, A. Muramatsu, and S. R. Manmana, Ground-state phase diagram of the one-dimensional t - J model, *Phys. Rev. B* **83**, 205113 (2011).
- [23] Z. Zhu, Q.-R. Wang, D. Sheng, and Z.-Y. Weng, Exact sign structure of the t - J chain and the single hole ground state, *Nucl. Phys. B* **903**, 51 (2016).
- [24] J. R. Coulthard, S. R. Clark, and D. Jaksch, Ground-state phase diagram of the one-dimensional $t - J$ model with pair hopping terms, *Phys. Rev. B* **98**, 035116 (2018).
- [25] J.-Y. Zhao, S. A. Chen, H.-K. Zhang, and Z.-Y. Weng, Two-hole ground state: Dichotomy in pairing symmetry, *Phys. Rev. X* **12**, 011062 (2022).
- [26] X. Deng, L. Wang, X. Dai, and Z. Fang, Local density approximation combined with gutzwiler method for correlated electron systems: Formalism and applications, *Phys. Rev. B* **79**, 075114 (2009).
- [27] Z. Ye, Y. Fang, H. Zhang, F. Zhang, S. Wu, W.-C. Lu, Y.-X. Yao, C.-Z. Wang, and K.-M. Ho, The gutzwiler conjugate gradient minimization method for correlated electron systems, *J. Phys. C: Condensed Matter* **34**, 243001 (2022).
- [28] F. D. M. Haldane, Luttinger liquid theory of one-dimensional quantum fluids. I. Properties of the Luttinger model and their extension to the general 1D interacting spinless Fermi gas, *J. Phys. C: Solid State Phys.* **14**, 2585 (1981).
- [29] Z. Y. Weng, D. N. Sheng, and C. S. Ting, Spin-charge separation in the t - J model: Magnetic and transport anomalies, *Phys. Rev. B* **52**, 637 (1995).
- [30] Z. Y. Weng, D. N. Sheng, Y.-C. Chen, and C. S. Ting, Phase string effect in the t - J model: General theory, *Phys. Rev. B* **55**, 3894 (1997).
- [31] M. Fishman, S. R. White, and E. M. Stoudenmire, The ITensor Software Library for Tensor Network Calculations, *SciPost Phys. Codebases*, 4 (2022).
- [32] M. Fishman, S. R. White, and E. M. Stoudenmire, Codebase release 0.3 for ITensor, *SciPost Phys. Codebases*, 4 (2022).
- [33] J.-Y. Zhao and Z.-Y. Weng, Mottness, phase string, and high- T_c superconductivity, *Chin. Phys. B* **31**, 087104 (2022).
- [34] J. Zhao, M. Thakurathi, M. Jain, D. Sen, and J. Jain, Density-functional theory of the fractional quantum hall effect, *Phys. Rev. Lett.* **118**, 196802 (2017).
- [35] Y. Hu and J. Jain, Kohn-Sham theory of the fractional quantum Hall effect, *Phys. Rev. Lett.* **123**, 176802 (2019).
- [36] Y. Hu, G. Murthy, S. Rao, and J. Jain, Kohn-Sham density functional theory of Abelian anyons, *Phys. Rev. B* **103**, 035124 (2021).
- [37] J. J. Moré, B. S. Garbow, and K. E. Hillstom, *User guide for MINPACK-1.[In FORTRAN]*, Tech. Rep. (Argonne National Lab.(ANL), Argonne, IL (United States), 1980).
- [38] P. Jordan and E. Wigner, Über das paulische Äquivalenzverbot, *Zeitschrift für Physik* **47**, 631 (1928).

APPENDIX I: PERFORMANCE OF THE CONVENTIONAL KS SCHEME

We have tested to apply the conventional KS scheme to solve the t - J model for several inhomogeneous density profiles. See Fig. 5 below for the calculation results. The KS results (grey curves) are found to significantly deviate from the DMRG (blue) and KS* (red) curves.

APPENDIX II: PERFORMANCE OF THE STANDARD MEAN-FIELD TREATMENT

Numerical comparisons between \hat{H}_{MF^*} and DMRG GS's on several inhomogeneous density profiles also indicate noticeable errors as shown in Fig. 6.

Analytically, we can show the failure of the standard mean-fied treatment in a simple example. Consider a homogeneous 4-site chain at half-filling under the open boundary condition. Since no holon is present, $h_i^\dagger h_{i+1} = 0$. The mean-field Hamiltonian becomes:

$$\hat{H}_{MF^*} = \sum_{\sigma} (t_1^f f_{1\sigma}^\dagger f_{2\sigma} + t_2^f f_{2\sigma}^\dagger f_{3\sigma} + t_3^f f_{3\sigma}^\dagger f_{4\sigma}) + H.c., \quad (15)$$

in which $t_i^f = -\frac{J}{2} \sum_{\sigma'} \langle f_{i,\sigma'}^\dagger f_{i+1,\sigma'} \rangle$. With the time-reversal symmetry, both spin states are equally occupied, and the inversion symmetry enforces $t_1^f = t_3^f$.

At half filling, we have 4 spinons to fully occupy the two lowest-energy single-particle states of \hat{H}_{MF^*} . Without loss of generality, we can write these two single-particle eigenvectors as:

$$\begin{aligned} |\psi_1\rangle &= \frac{1}{\sqrt{2}} (\cos \theta, \sin \theta, \sin \theta, \cos \theta) \\ |\psi_2\rangle &= \frac{1}{\sqrt{2}} (\sin \theta, \cos \theta, -\cos \theta, -\sin \theta), \end{aligned} \quad (16)$$

which lead to

$$\begin{aligned} t_1^f &= -J \cos \theta \sin \theta = -\frac{J}{2} \sin(2\theta) \\ t_2^f &= -\frac{J}{2} (\sin^2 \theta - \cos^2 \theta) = \frac{J}{2} \cos(2\theta). \end{aligned} \quad (17)$$

The solutions for Eqs. (15-17) to be self-consistent are:

$$\theta = \frac{(2N+1)\pi}{4}, N \in Z. \quad (18)$$

Accordingly, $t_2^f = 0$, the chain is decoupled into two dimers. This example shows that the standard mean-field treatment predicts a wrong valence-bond-solid spin state.

APPENDIX III: LDA DESIGN OF THE DENSITY FUNCTIONS

The mean-field treatment is best applied to infinitely-long homogeneous chains with dilute holes. We will use the MF formula near $n=1$ as a guide to design the LDA functions.

For a N_s -site homogeneous chain under the periodic boundary condition, we have:

$$\begin{aligned} \langle h_i^\dagger h_{i+1} \rangle &= \frac{1}{2N_s} \sum_i (\langle h_i^\dagger h_{i+1} \rangle + H.c.) \\ &= \frac{1}{2N_s^2} \sum_{ikk'} (\langle h_k^\dagger e^{ikr_i} h_{k'} e^{-ik'r_{i+1}} \rangle + H.c.) \\ &= \frac{1}{2N_s} \sum_{kk'} (\langle e^{-ik'} h_k^\dagger h_{k'} \sum_i \frac{1}{N_s} e^{i(k-k')r_i} \rangle + H.c.) \\ &= \frac{1}{2N_s} \sum_{kk'} (\langle e^{-ik'} h_k^\dagger h_{k'} \delta_{k,k'} \rangle + H.c.) \\ &= \frac{1}{N_s} \sum_k \langle \cos(k) h_k^\dagger h_k \rangle \\ &= \frac{1}{N_s} \sum_{k \in occ.} \cos(k) \\ &= \frac{1}{2\pi} \sum_{k \in occ.} \cos(k) \Delta k \\ &= \frac{1}{2\pi} \int_{-k_{max}}^{k_{max}} \cos(k) dk \\ &= \frac{\sin(k_{max})}{\pi} \\ &= \frac{1}{\pi} \sin(\pi(1-n)), \end{aligned} \quad (19)$$

in which the real-space quantity is Fourier transformed to the k -space by summing up all the occupied Bloch states, and the sum is converted to an integral by taking the $N_s \rightarrow \infty$ limit. The largest occupied $|k|$ associates with the electron density $n \in [0, 1]$ as $|k_{max}| = \pi(1-n)$:

$$\frac{N_s}{2\pi} \int_{-k_{max}}^{k_{max}} dk = N_h = N_s - N_e \quad (20)$$

Similarly,

$$\begin{aligned} \langle f_{i\sigma}^\dagger f_{i+1\sigma} \rangle &= \frac{\sin(k_{max})}{\pi} \\ &= \frac{\sin(n\pi/2)}{\pi}, \end{aligned} \quad (21)$$

in which k_{max} is determined by

$$\frac{N_s}{2\pi} \int_{-k_{max}}^{k_{max}} dk = \frac{N_e}{2}. \quad (22)$$

The expression differs from that of holons because of the extra spin degree of freedom and the particle number constraint.

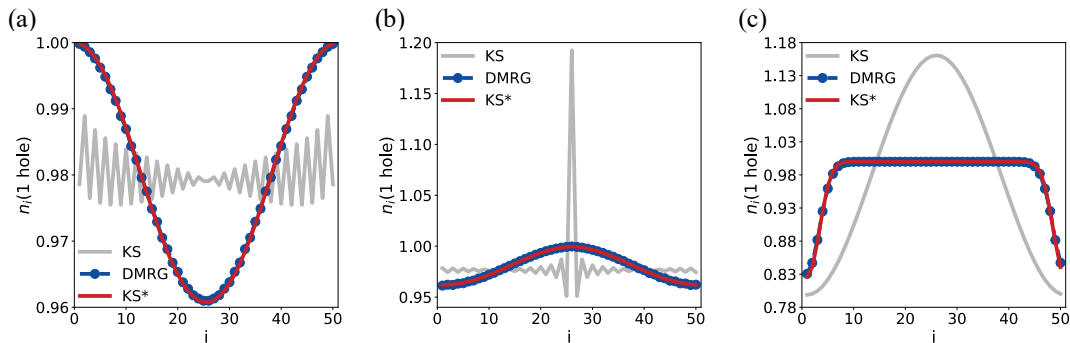


FIG. 5. Comparison of the KS results with respect to the 1-hole density distributions of a 50-site chain (a) under the open boundary condition; (b) under the periodic boundary condition and subject to a single-site impurity potential $V_{imp} = -1$; (c) under the periodic boundary condition and subject to a periodic potential $V_i = \cos(2\pi i/N_p)$.

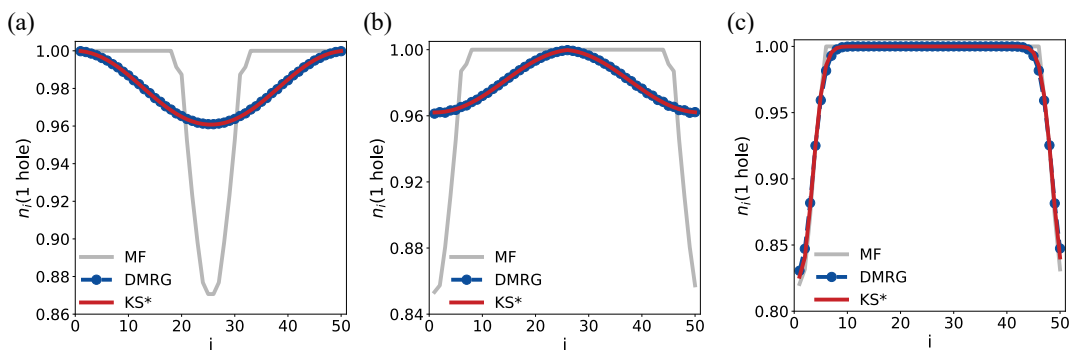


FIG. 6. Comparison of the MF results with respect to the 1-hole density distributions of a 50-site chain (a) under the open boundary condition; (b) under the periodic boundary condition and subject to a single-site impurity potential $V_{imp} = -1$; (c) under the periodic boundary condition and subject to a periodic potential $V_i = \cos(2\pi i/N_p)$.

The practical LDA constructions employed in the main context can be regarded as the lowest-order expansion around $n = 1$ with two empirically chosen expansion coefficients, which are found to give better numerical results than the original nonmonotonic trigonometric functions. Tuning the expansion coefficients can be viewed as a renormalization of the hopping amplitudes of the fractionalized particles. This defines different versions of the noninteracting auxiliary systems. In Fig. 7, we plot t_{KS^*} and ε_{xc^*} obtained from several values of the expansion coefficients A and B , as well as from the rigorous mean-field definition of $\langle h_i^\dagger h_{i+1} \rangle$ and $\langle f_{i\sigma}^\dagger f_{i+1\sigma} \rangle$. Note that for homogeneous chains, they all consistently reproduce the exact GS energy. Testing calculations on inhomogeneous chains show that $A = 0.45$ and $B = -0.05$ generally perform well. A phenomenological understanding is that this choice makes t_{KS^*} captures a predominant part of ε_{GS} , and ε_{xc^*} shows a simple linear dependence on n .

APPENDIX IV: CODE IMPLEMENTATION AND AVAILABILITY

The DMRG calculations are conducted using the ITensors Library [31, 32]. We retain up to 1600 states to control truncation errors up to the order of 10^{-12} over 25 sweeps, demonstrating excellent convergence.

The KS* code used to generate our data is available at: <https://github.com/Promebo/fractional-KS>. The algorithm contains two self-consistent loops. The outer loop is the standard DFT density iteration. We employ the simple linear mixing method: $n_i^{new} = \gamma n_i^{input} + (1 - \gamma)n_i^{output}$. We fix γ to be 0.4 for all the calculations. The inner loop is to search for local chemical potentials λ_i , which appear in the last term of \hat{H}_{KS^*} , such that the GS satisfies $\langle h_i^\dagger h_i + \sum_{\sigma} f_{i\sigma}^\dagger f_{i\sigma} - 1 \rangle = 0$. We employ the modified Powell method [37] to iteratively determine λ_i as roots of non-linear equations. The abrupt occupancy change around the Fermi surface of the fractionalized particles tend to result in oscillations in the

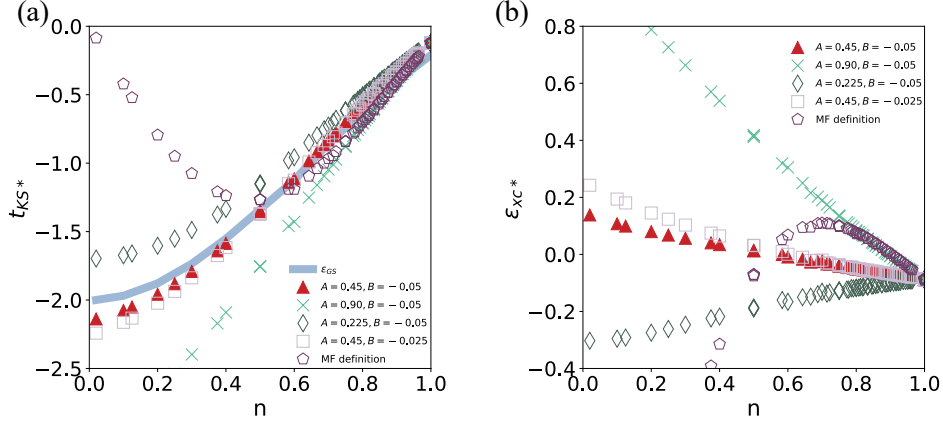


FIG. 7. Homogeneous density dependence of (a) t_{KS^*} and (b) ϵ_{xc^*} with different A and B, as well as from the rigorous mean-field definition of $\langle h_i^\dagger h_{i+1} \rangle$ and $\langle f_{i\sigma}^\dagger f_{i+1\sigma} \rangle$. In (a), the DMRG GS energy (ϵ_{GS}) is plotted as the benchmark.

iterations, similar to the metal convergence problem in electron DFT. To accelerate the convergence, we introduce Gaussian smearing.

As the basis of the KS^* scheme, the fractionalization construction [17] formally relates the holon and spinon operators to the electron operators as $c_{i\sigma} = h_i^\dagger f_{i\sigma}$. To keep the fermionic statistics of electrons, we assign $f_{i\sigma}$ (spinon) as a fermion operator and h_i (holon) as a hard-core boson operator. In 1D, the hard-core bosons can also be converted to fermions via the Jordan-Wigner transformation [38]. Therefore, in practice, both the spinon and holon eigenstates can be conveniently solved by matrix diagonalization.

With respect to the holon operators, the transformation is defined as:

$$\begin{aligned} \mathfrak{h}_i &= \exp(i\pi \sum_{j=1}^{i-1} \hat{n}_j) h_i \\ \mathfrak{h}_i^\dagger &= \exp(-i\pi \sum_{j=1}^{i-1} \hat{n}_j) h_i^\dagger, \end{aligned} \quad (23)$$

where $\hat{n}_j = h_j^\dagger h_j$ is holon number operator. Thus transformed $\mathfrak{h}_i, \mathfrak{h}_i^\dagger$ satisfy the fermion anticommutation relations.

We also have the following relations:

$$\begin{aligned} h_i^\dagger h_i &= \mathfrak{h}_i^\dagger \mathfrak{h}_i \\ h_i^\dagger h_{i+1} &= \mathfrak{h}_i^\dagger \mathfrak{h}_{i+1}. \end{aligned} \quad (24)$$

For a N_s -site chain under periodic boundary conditions, there is an additional boundary hopping term:

$$h_{N_s}^\dagger h_1 = e^{i\pi(N_h+1)} \mathfrak{h}_{N_s}^\dagger \mathfrak{h}_1, \quad (25)$$

in which N_h is the total holon number. Note that if N_h is even, a minus sign will appear for this hopping term.

APPENDIX V: ADDITIONAL CALCULATION RESULTS

Fig. 8 contains the multi-hole energy analysis of the t - J model. For all the calculated cases, the KS^* scheme is able to accurately reproduce the GS energies.

Similar to the conventional Kohn-Sham scheme, although there is no guarantee that physical properties other than the GS density and energy can be correctly reproduced, all the correlation functions are practically calculable based on the noninteracting auxiliary system. The results should contain important features, but errors are also expected.

We first show in Fig. 9(a) the single-particle correlation $\langle c_{i\sigma}^\dagger c_{j\sigma} \rangle$, which forms the basis to calculate other correlation functions within the KS^* scheme. The spin-charge fractionalization translates this quantity into $\langle h_j^\dagger h_i \rangle \langle f_{i\sigma}^\dagger f_{j\sigma} \rangle$. The KS^* scheme provides noninteracting holon and spinon wavefunctions, so the calculation can be easily implemented. In comparison to DMRG, the general trend is nicely captured, but the amplitude is clearly underestimated.

The spin-spin correlation $\langle S_i^z S_j^z \rangle$ is calculated as:

$$\begin{aligned} \langle S_i^z S_j^z \rangle &= \frac{1}{4} \langle (f_{i\uparrow}^\dagger f_{i\uparrow} - f_{i\downarrow}^\dagger f_{i\downarrow}) \times (f_{j\uparrow}^\dagger f_{j\uparrow} - f_{j\downarrow}^\dagger f_{j\downarrow}) \rangle \\ &= \frac{1}{4} (\langle f_{i\uparrow}^\dagger f_{i\uparrow} \rangle - \langle f_{i\downarrow}^\dagger f_{i\downarrow} \rangle) \times (\langle f_{j\uparrow}^\dagger f_{j\uparrow} \rangle - \langle f_{j\downarrow}^\dagger f_{j\downarrow} \rangle) - \\ &\quad \frac{1}{4} \sum_{\sigma} \langle f_{i\sigma}^\dagger f_{j\sigma} \rangle \langle f_{j\sigma}^\dagger f_{i\sigma} \rangle + \frac{1}{4} \sum_{\sigma} \langle f_{i\sigma}^\dagger f_{j-\sigma} \rangle \langle f_{j-\sigma}^\dagger f_{i\sigma} \rangle \end{aligned}$$

Within the current (nonmagnetic) KS^* scheme, the term in the second row and the last term in the third row are

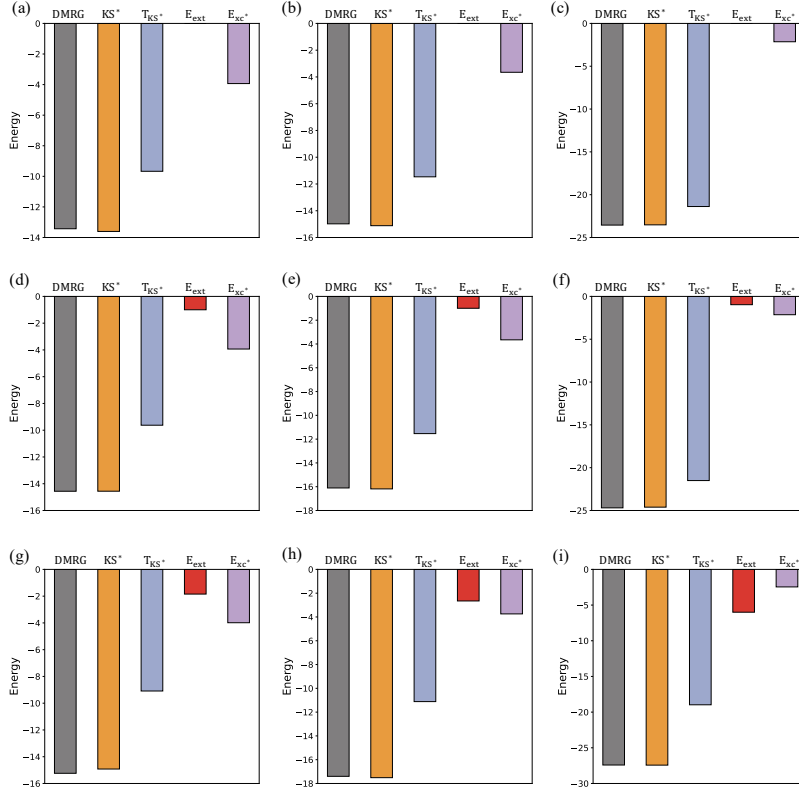


FIG. 8. The 2-, 3-, and 9-hole GS energy and the decomposition into T_{KS^*} , E_{xc^*} and $E_{ext} \equiv \sum_i V_i n_i$ within the KS^* scheme of (a-c) a 50-site OBC chain; (d-f) a 50-site PBC chain subject to a single-site impurity potential $V_{imp} = -1$; and (g-i) a 50-site PBC chain subject to a periodic potential $V_i = \cos(2\pi i/N_p)$.

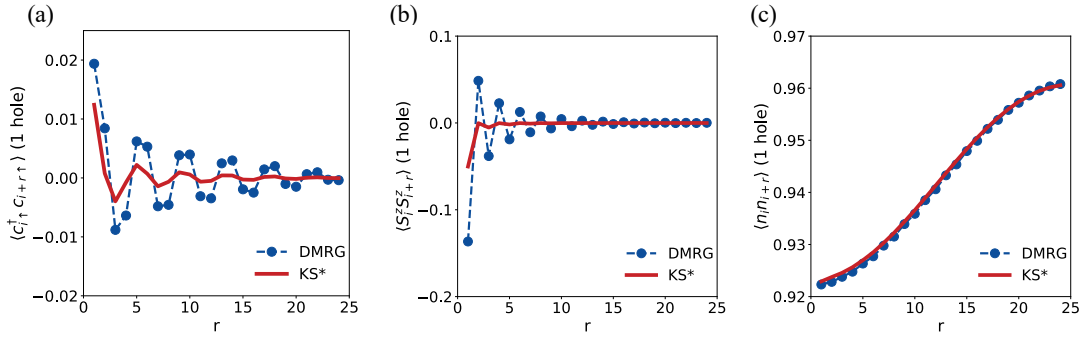


FIG. 9. Correlation functions of a t - J chain (50 sites, 1 hole, open boundary condition). (a) $\langle c_{i\uparrow}^\dagger c_{i+r\uparrow} \rangle$, (b) $\langle S_{i\uparrow}^z S_{i+r\downarrow}^z \rangle$ and (c) $\langle n_i n_{i+r} \rangle$; i is chosen to be the center of the chain and r is the distance.

both zero. The results are shown in Fig. 9(b). In comparison to DMRG, the amplitude error occurring at the single-particle correlation level is further enhanced. Nevertheless, one important feature is captured, namely the odd-even oscillation, which signifies the tendency to anti-ferromagnetism. It is possible to improve the description in the future by improving the nonmagnetic LDA to the spin-dependent level.

One important correlation function is in principle ex-

act within the KS^* ansatz, i.e. the density-density correlation, which characterizes the key Luttinger parameter (commonly termed as K_ρ [16]). It can be calculated as:

$$\begin{aligned} \langle n_i n_j \rangle &= \langle (1 - h_i^\dagger h_i)(1 - h_j^\dagger h_j) \rangle \\ &= 1 - \langle h_i^\dagger h_i \rangle - \langle h_j^\dagger h_j \rangle + \langle h_i^\dagger h_i \rangle \langle h_j^\dagger h_j \rangle - \langle h_i^\dagger h_j \rangle \langle h_j^\dagger h_i \rangle. \end{aligned}$$

We show in Fig. 9(c) that the KS^* results indeed yield excellent agreement with DMRG.

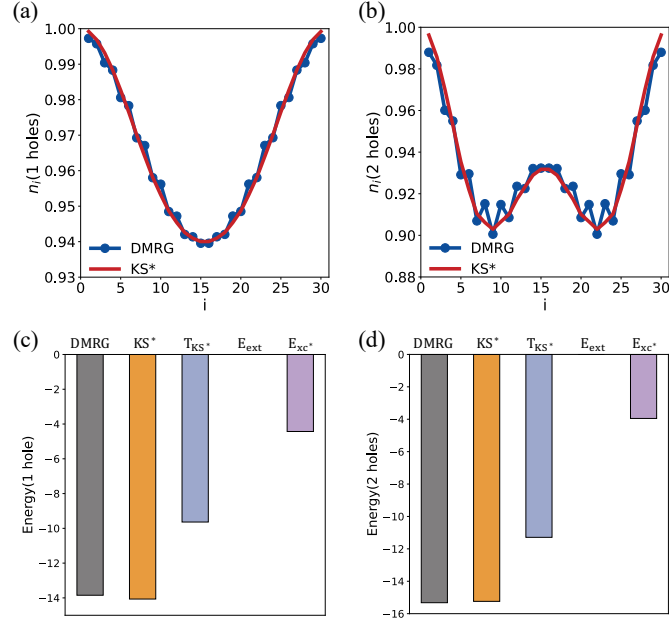


FIG. 10. Testing calculations on a 30-site 1D Hubbard chain ($U=6$, open boundary conditions). (a,b) Density distribution under one-hole doping ($N_e=29$) and two-hole doping ($N_e=28$); (c ,d) GS energy and its decomposition within the KS* scheme corresponding to the uppers panels. The LDA parameters are set to be $A = 0.35$, $B = -0.05$, and $\epsilon_{xc^*} = -0.35n + 0.19$. The KS* computational procedure is identical to that used for the t - J chain.

Since the Luttinger liquid behavior is a common feature of interacting electrons in 1D, the KS* construction demonstrated in the present work in terms of spin-charge

separation has certain “1D universal applicability”. Fig. 10 shows testing calculation results on a 1D Hubbard model with minimal modifications of the LDA parameters.